

Heliospheric, Astropheric, and Interstellar Lyman- α Absorption Toward 36 Oph¹

Brian E. Wood, Jeffrey L. Linsky

JILA, University of Colorado, and NIST, Boulder, CO 80309-0440.

woodb@marmot.colorado.edu, jlinsky@jila.colorado.edu

and

Gary P. Zank

Bartol Research Institute, University of Delaware, Newark, DE 19716.

zank@bartol.udel.edu

ABSTRACT

We use high-resolution UV spectra taken by the Space Telescope Imaging Spectrograph instrument on board the *Hubble Space Telescope* to study the 5.5 pc line of sight to the K0 V star 36 Oph A. The one interstellar component detected for this line of sight has a velocity inconsistent with the local interstellar cloud (LIC) flow vector, but consistent with the flow vector of the so-called G cloud, a very nearby warm cloud in the Galactic Center direction. From our data, we measure the following values for the interstellar temperature, nonthermal velocity, H I column density, and D/H value: $T = 5900 \pm 500$ K, $\xi = 2.2 \pm 0.2$ km s⁻¹, $\log N_{\text{H}} = 17.85 \pm 0.15$, and $\text{D/H} = (1.5 \pm 0.5) \times 10^{-5}$. The temperature of the G cloud is somewhat lower than that of the LIC, and Mg and Fe depletions are also lower, but the D/H value appears to be the same. Based on upper limits for the LIC absorption, we estimate the distance to the edge of the LIC to be $d_{\text{edge}} < 0.19$ pc, which the Sun will reach in $t_{\text{edge}} < 7400$ yrs.

The H I Lyman- α absorption line has properties inconsistent with those of the other absorption lines, indicating the presence of one or more absorption components not seen in the other lines. We present evidence that hot neutral hydrogen local to both the Sun and the star is responsible for the excess Lyman- α absorption. This hot H I is created by the interaction between the ISM and the winds of the Sun and 36 Oph A. The observed line of sight lies only 12° from the upwind direction of the LIC flow vector, where hydrodynamic models of the heliosphere suggest that heliospheric H I absorption

¹Based on observations with the NASA/ESA Hubble Space Telescope, obtained at the Space Telescope Science Institute, which is operated by the Association of Universities for Research in Astronomy, Inc., under NASA contract NAS5-26555.

should be particularly prominent. The properties of the heliospheric absorption ($T = 38,000 \pm 8000$ K and $\log N_{\text{H}} = 14.6 \pm 0.3$) are consistent with previous measurements of this absorption for the α Cen line of sight 52° from the upwind direction.

Subject headings: ISM: atoms — solar wind — stars: individual (36 Oph A) — stars: winds, outflows — ultraviolet: ISM

1. Introduction

In 1996, high quality spectra of the very nearby star α Cen taken by the Goddard High Resolution Spectrograph instrument on board the *Hubble Space Telescope* (HST) yielded a serendipitous detection of neutral hydrogen in the outer heliosphere (Linsky & Wood 1996, hereafter LW96), thereby providing a unique new way to observationally study the structure and internal properties of the heliosphere. Previous studies of heliospheric neutral hydrogen had relied primarily on Lyman- α backscatter measurements, which are mostly sensitive to very nearby H I (Bertaux et al. 1985; Quémérais et al. 1995). In the α Cen data, the heliospheric H I produces an absorption signature in the stellar Lyman- α line that allows it to be detected despite being highly blended with absorption from the local interstellar medium (LISM). LW96 demonstrated that the properties of the heliospheric H I inferred from the data are consistent with the predictions of heliospheric models (Baranov & Malama 1993, 1995; Pauls, Zank, & Williams 1995; Zank et al. 1996; Zank 1999). Gayley et al. (1997) confirmed this result by directly comparing the data with H I absorption predicted by the models, and they also found evidence that H I in the “astrosphere” of α Cen is also accounting for some of the non-LISM absorption observed in the Lyman- α line.

The α Cen line of sight lies 52° from the upwind direction of the interstellar flow through the heliosphere. In the upwind side, the heliospheric H I absorption is expected to be dominated by neutral hydrogen in the “hydrogen wall” (or “H-wall” for short), located between the heliopause and solar bow shock. In this region, interactions with solar wind protons heat and decelerate the plasma component of the interstellar wind. Charge exchange with this plasma then heats, compresses, and decelerates the neutral hydrogen as well. The high temperature and decelerated velocity of the H I in the hydrogen wall both play important roles in allowing absorption from this material to be detectable despite being blended with an LISM absorption component with a much larger column density. The high temperature broadens the H-wall absorption substantially, and the deceleration shifts the absorption away from the LISM absorption, resulting in a noticeable excess of Lyman- α absorption on the red side of the line.

The deceleration should be at its largest in the upwind direction, so the Lyman- α signature of the H-wall should become even easier to detect if one looks closer to the upwind direction than the α Cen line of sight 52° away. Thus, we searched for another target for HST that would be much closer to the upwind direction. We chose the nearby ($d = 5.5$ pc) K0 V star 36 Oph A (=HD 155886), which is only 12° from the upwind direction. Our main goals in observing this star are to

confirm the detection of the solar hydrogen wall claimed in the analysis of the α Cen data, and to provide additional constraints on the properties of the H-wall.

2. Observations and Data Reduction

On 1999 October 10, we observed 36 Oph A with the Space Telescope Imaging Spectrograph (STIS) instrument on HST. The STIS instrument is described in detail by Kimble et al. (1998) and Woodgate et al. (1998). We observed the 1160 – 1357 Å spectral region with the high-resolution E140H grating and $0.2'' \times 0.2''$ aperture, and we used two exposures with the E230H grating and $0.1'' \times 0.2''$ aperture to observe the 2430 – 2943 Å spectral range. The former region contains the Lyman- α line at 1216 Å that is of primary interest to us, while the latter region contains interstellar lines of Mg II and Fe II. These metal lines provide important information on the properties of the LISM that can be used to constrain the LISM H I Lyman- α absorption, making it easier to separate it from the heliospheric absorption.

The data were reduced using the STIS team’s CALSTIS software package written in IDL (Lindler 1999). The reduction included assignment of wavelengths using calibration spectra obtained during the course of the observations. A substantial amount of scattered light was clearly present in the saturated core of the Lyman- α line. This flux was removed from the data using the ECHELLE_SCAT routine in the CALSTIS package. A geocoronal Lyman- α emission feature in the middle of the interstellar H I absorption was fitted with a Gaussian, and then removed by subtracting the fitted Gaussian from the data. The centroid of the Gaussian is at -26.6 km s^{-1} , which agrees very well with the expected location of -26.4 km s^{-1} based on the Earth’s projected velocity toward the star at the time of observation. This confirms the accuracy of our wavelength calibration.

3. Data Analysis

3.1. Single Component Fits

Besides H I Lyman- α at 1215.670 Å, there are only four interstellar absorption features apparent in our data that can be accurately measured: D I Lyman- α λ 1215.339, Fe II λ 2600.173, and the Mg II h & k lines at 2803.531 Å and 2796.352 Å, respectively. The rest wavelengths quoted above are vacuum wavelengths. These lines are all shown in Figure 1.

None of the lines in Figure 1 show any asymmetries that would indicate the presence of more than one absorption component, so all are fitted with a single component. The dotted lines in the figure are the fits before correction for instrumental broadening, and the thick solid lines that fit the data are the fits after the instrumental broadening correction is applied. The line spread functions used in these corrections were taken from Sahu et al. (1999). The oscillator absorption strengths

assumed in our fits are from Morton (1991). The parameters of the fits are listed in Table 1.

In order to constrain the Mg II fits as much as possible, the 2 Mg II lines were fitted simultaneously with both lines forced to have the same column density (N), Doppler parameter (b), and central velocity (v). We were concerned about the possibility that much of the residual flux present below the Mg II absorption lines may be scattered light. Unfortunately, there is currently no scattered light correction for E230H data like there is for E140H spectra (see above). We tried fits with much of the possible scattered light flux subtracted from the spectrum to see the degree to which the fit parameters were affected. The uncertainties quoted in Table 1 include the systematic uncertainties we estimate due to the uncertain scattered light correction.

Both LISM studies and *in situ* measurements of LISM material within the solar system suggest that the velocity of the incoming interstellar wind is about 26 km s^{-1} (Witte et al. 1993; Lallement et al. 1995). However, the LISM flow vector appears to be different for lines of sight toward the Galactic center, with a faster speed of 29.4 km s^{-1} . Thus, it has been proposed that a different cloud lies in this direction, the so-called G cloud (Lallement & Bertin 1992). If this interpretation is correct the Sun must be very near the edge of the Local Interstellar Cloud (LIC), since all the LISM absorption detected by LW96 toward α Cen (which is roughly in the Galactic center direction) is at the expected velocity of the G cloud and none is at the velocity predicted for that line of sight by the LIC vector (see also Lallement et al. 1995).

The outlines of the LIC and the G cloud in the Galactic plane are shown in Figure 2, as are the projected locations of the Sun, α Cen, and 36 Oph. The LIC outline is from Redfield & Linsky (2000). The G cloud shape is not well known, so the contour shown in Figure 2 is only a crude but plausible representation for this cloud. The velocity vectors of the LIC and G clouds are also shown in the figure.

With Galactic coordinates of $l = 358^\circ$, $b = 7^\circ$; 36 Oph lies almost directly toward the Galactic center, very near the upwind directions of both the LIC and G cloud vectors. The flow velocities predicted for the 36 Oph line of sight by these two vectors are -25.1 and -28.4 km s^{-1} , respectively. The LISM velocity measured toward 36 Oph agrees very well with the latter velocity (see Table 1), so we conclude that all of the LISM absorption we detect is from the G cloud. Inspection of Figure 1 reveals that there is no visible absorption component centered at the LIC velocity. Thus, our findings are very similar to those of LW96. However, the evidence for higher flow velocities toward the Galactic Center, and the close proximity of the edge of the LIC, is particularly striking in our data, because even the *projected* LISM velocities that we directly observe are larger than the 26 km s^{-1} velocity that has been measured for the LIC.

We now try to estimate how far the Sun is from the edge of the LIC. We need to first estimate an upper limit for the H I column density, and the best way to do this is to determine upper limits for the D I and/or Mg II column densities and then calculate the H I upper limit based on the known abundance ratios in the LIC. For both D I and Mg II we repeat the fits shown in Figure 1, but with added LIC absorption components centered on the known LIC velocity and with

Doppler parameters consistent with previous observations of LIC material ($b_{\text{D I}} = 8.2 \text{ km s}^{-1}$ and $b_{\text{Mg II}} = 3.0 \text{ km s}^{-1}$). We experiment with different LIC/G cloud column density ratios to see at what point we believe the fits become unacceptable.

One might think that the Mg II lines would provide the best constraints because they are narrower and more optically thick than D I. However, the D I/Mg II ratio is larger in the LIC than in the G cloud by about a factor of 4 (see below). Based on experiments with different D I fits, we estimate that the D I column density of the LIC is no more than 10% that of the G cloud, corresponding to an upper limit of $N_{\text{D I}} < 9 \times 10^{11} \text{ cm}^{-2}$. Note that this corresponds to a LIC contribution of 2.5% to the Mg II lines. For LIC contributions greater than this, the χ^2_ν values of the fits become significantly worse, and the G cloud D I absorption becomes more and more blueshifted away from the expected velocity of the G cloud. (If we force it to be at the expected velocity, the quality of the fit degrades even more.)

The LIC D/H value is 1.5×10^{-5} (Linsky 1998; Linsky & Wood 1998), so $N_{\text{H I}} < 6 \times 10^{16} \text{ cm}^{-2}$ for the LIC. Assuming a density of $n_{\text{H I}} = 0.10 \text{ cm}^{-3}$ (Linsky et al. 2000), the upper limit for the distance to the edge of the LIC is $d_{\text{edge}} < 0.19 \text{ pc}$ for the 36 Oph line of sight, consistent with the $d_{\text{edge}} = 0.05 \text{ pc}$ value suggested by the LIC model of Redfield & Linsky (2000) (see Fig. 2). The LIC material is moving toward the Sun with a velocity of -25.1 km s^{-1} along this line of sight, so we will reach the edge in $t_{\text{edge}} < 7400 \text{ yrs}$.

The Doppler parameters (b) listed in Table 1 are related to the temperature, T , and nonthermal velocity, ξ , by the following equation:

$$b^2 = 0.0165 \frac{T}{A} + \xi^2, \quad (1)$$

where b and ξ are in units of km s^{-1} , and A is the atomic weight of the element in question. In Figure 3, the measured Doppler parameters of the Mg II, Fe II, and D I lines are used with equation (1) to derive curves of ξ vs. T , with error bars. The shaded region in the figure is the area of overlap for these curves, which identifies the temperature and ξ values for the observed LISM material.

Our measured temperature and nonthermal velocity based on this analysis are $T = 5900 \pm 500 \text{ K}$ and $\xi = 2.2 \pm 0.2 \text{ km s}^{-1}$. This temperature is consistent with the $T = 5400 \pm 500 \text{ K}$ temperature observed toward α Cen, supporting the assertion of LW96 that the G cloud temperature is somewhat cooler than the LIC temperature of $T = 8000 \pm 1000 \text{ K}$ (Dring et al. 1997; Piskunov et al. 1997; Wood & Linsky 1998). However, the nonthermal velocity toward 36 Oph appears to be somewhat larger than that observed toward α Cen ($\xi = 1.25 \pm 0.25 \text{ km s}^{-1}$).

The relative abundances of D I, Mg II, and Fe II suggested by the column densities in Table 1 are consistent with the α Cen measurements. These results suggest that Mg and Fe are less depleted in the G cloud than in the LIC. For example, the D I/Mg II ratio is 0.9 ± 0.4 toward 36 Oph and 1.2 ± 0.2 toward α Cen, but is ≥ 4 for the LIC (LW96; Dring et al. 1997; Piskunov et al. 1997), with the apparent exception of the Sirius line of sight which has a D I/Mg II ratio of about 1.7 (Lallemand et al. 1994; Bertin et al. 1995).

In Figure 4, we present our single component fit to the H I Lyman- α line, combined with the D I Lyman- α fit from Figure 1. The parameters of the H I fit are provided in Table 1. In constructing this fit, we started with an assumed stellar Lyman- α profile based on a broadened version of the observed Mg II k line profile. We then performed an initial fit, altered the assumed stellar profile to improve the quality of the fit, and then attempted another fit. Yet another iteration of this process was required before arriving at the fit in Figure 4.

This Lyman- α fitting technique has been used in many past analyses (LW96; Piskunov et al. 1997; Wood & Linsky 1998). The argument for using the Mg II line as a starting point is that the Mg II k and Lyman- α lines are both highly optically thick chromospheric lines that have similar shapes in the solar spectrum. It should be stated, however, that for single component fits it actually matters little what initial model is used for the stellar Lyman- α profile. The initial profile is altered significantly before the final best fit is determined, and the final fit parameters are therefore independent of the initial assumptions about the shape of the stellar profile. This was demonstrated clearly in the α Cen analysis, where the Lyman- α lines of both members of the α Cen binary system were independently fitted with single absorption components and the derived interstellar parameters were the same (LW96).

The residuals of the single component H I fit in Figure 4 suggest some minor systematic discrepancies, but the quality of the fit is not too bad. However, the main problem with the fit is that the velocity and Doppler parameter of the H I absorption are completely inconsistent with those of the other lines, D I in particular (see Table 1). The central velocity of H I is -25.9 km s^{-1} , as opposed to the -28.4 km s^{-1} average velocity observed for the other lines. The Doppler parameter of H I (14.34 km s^{-1}) suggests temperatures of about 12,000 K, compared with the $\sim 6000 \text{ K}$ temperature determined mostly from D I (see Fig. 3). If a curve was plotted in Figure 3 for H I it would be a nearly vertical line centered at about 12,000 K, which actually lies off the right edge of the figure, emphasizing just how discrepant H I is relative to D I and the other lines.

These problems with H I are very reminiscent of those found for the α Cen line of sight (LW96). Collectively they represent the primary piece of evidence for a hydrogen wall contribution to the Lyman- α absorption toward both α Cen and 36 Oph, because the only way to resolve the discrepancies is to add a second absorption component to the H I fit with properties that turn out to be consistent with those expected for the solar H-wall. The H I Lyman- α line of α Cen exhibits a $+2.2 \text{ km s}^{-1}$ velocity discrepancy and about a $+3000 \text{ K}$ temperature discrepancy relative to the other lines (LW96). The 36 Oph discrepancies are in the same direction, but are even larger ($+2.5 \text{ km s}^{-1}$ and $+6000 \text{ K}$). This is consistent with our expectations, since the H-wall closer to the upwind direction should be more decelerated and may be a bit hotter (see, e.g., Zank et al. 1996).

Since the LIC velocity is redshifted relative to the G cloud velocity, one might wonder if LIC H I absorption might be responsible for the velocity discrepancy between H I and the other lines. In Figure 4 we show the LIC absorption associated with the $N_{\text{H}} < 6 \times 10^{16} \text{ cm}^{-2}$ upper limit derived above (dotted line). Essentially all of the LIC absorption is well within the saturated core of the

line, so the LIC will not have any observable effect on the Lyman- α line.

3.2. The Bisector Technique

Although single component H I fits are unique and well-constrained, this is not necessarily the case for two component fits, as LW96 demonstrated in the α Cen analysis. Thus, before attempting a two component fit, we try to constrain the LISM H I column density by other means. Wood, Alexander, & Linsky (1996) measured an LISM column density toward ϵ Indi by determining the amount of absorption in the wings of the Lyman- α line, based on the assumption that the far wings of the stellar Lyman- α profile should be centered on the rest frame of the star, as is the case for the Sun. This “bisector technique” only works when there is a substantial wavelength difference between the LISM absorption and the center of the stellar Lyman- α line, creating a situation where there is more absorption in one wing than the other. This induces an apparent line shift in the wings, the magnitude of which is dependent on the LISM column density. This analysis technique could not be tried in the α Cen analysis, since there is no significant shift between the stellar emission and LISM absorption, but in our 36 Oph data there is about a 30 km s^{-1} shift between the two.

The bisector technique relies on an accurate stellar radial velocity. The radial velocity listed for 36 Oph in the literature is -1 km s^{-1} (Hirshfeld, Sinnott, & Ochsenbein 1996). However, all the chromospheric lines in our spectra, including Mg II h & k and the O I triplet at 1300 \AA , are centered on $+1.0 \text{ km s}^{-1}$. Thus, we believe this is a more likely value for the radial velocity, and in any case a far more likely value for the centroid of the Lyman- α wings. Since 36 Oph A is a member of a binary system, we speculate that perhaps orbital motion has changed the stellar velocity from the systemic value of -1 km s^{-1} . Based primarily on the centroids of the Cl I $\lambda 1351.657$ and O I] $\lambda 1355.598$ lines, which can be measured very accurately because of the very narrow line widths of these features ($FWHM \sim 0.04 \text{ \AA}$), we assume a velocity of $+1.0 \pm 0.2 \text{ km s}^{-1}$ for the star. Since other chromospheric lines in our spectra have this centroid velocity, including Mg II h & k, it is reasonable to assume the far wings of Lyman- α , which are formed at the base of the chromosphere, will have it too.

Figure 5 shows how the analysis technique works. First, we fit polynomials to the wings of the observed Lyman- α line, interpolating over the D I line. Working from these fits (thick solid lines in Fig. 5a), we can derive what the wings of the stellar Lyman- α line would look like assuming different values of the H I column density. The results for five different column densities are shown in Figure 5a. In Figure 5b we display the bisectors of these wings for various values of $\log N_{\text{H}}$. As the column density increases the bisectors become more and more blueshifted, due to the fact that the LISM is absorbing more in the blue wing of the line than in the red wing.

Ideally, a vertical bisector centered at the radial velocity of the star should result when the correct value of $\log N_{\text{H}}$ is assumed, but in practice this does not happen due to uncertainties in

the polynomial fits to the data and in measuring the location of the bisectors. Nevertheless, in Figure 5b we identify with a solid line the bisector that we believe best matches the stellar radial velocity of $+1.0 \text{ km s}^{-1}$, which corresponds to $\log N_{\text{H}} = 17.84$. Column densities in the range $\log N_{\text{H}} = 17.7 - 18.0$ all produce bisectors with average velocities within about $\pm 1 \text{ km s}^{-1}$ of the expected velocity, so we decide on a value of $\log N_{\text{H}} = 17.85 \pm 0.15$ for our best estimate of the LISM H I column density toward 36 Oph.

This range of columns yields deuterium-to-hydrogen ratios in the range $D/\text{H} = (1.0 - 2.0) \times 10^{-5}$, so we quote a value of $D/\text{H} = (1.5 \pm 0.5) \times 10^{-5}$. This is an encouraging result, since it is consistent with the mean value $D/\text{H} = (1.5 \pm 0.1) \times 10^{-5}$ for the LIC (Linsky 1998; Linsky & Wood 1998). The error bars in the G cloud D/H value are too large to tell if it is actually identical to the LIC value, but apparently the G cloud does not have a drastically different D/H value than the LIC.

3.3. Multi-Component Fits

In Figure 6a, we present a two component fit to the Lyman- α line, where the dotted line represents LISM absorption and the dashed line represents absorption from the solar hydrogen wall. The LISM component is forced to have the average velocity observed for the other LISM lines ($v = -28.4 \text{ km s}^{-1}$) and a Doppler parameter derived from the T and ξ values measured from the other lines ($b = 10.11 \text{ km s}^{-1}$). Only a single two component fit is shown in Figure 6, but in practice we performed many fits assuming different stellar Lyman- α profiles that allowed the LISM H I column density to vary within the $\log N_{\text{H}} = 17.7 - 18.0$ range allowed by the bisector analysis. This experimentation allowed us to better determine the best fit parameters and their uncertainties, which are listed in Table 1.

The quality of the two component fit is certainly better than the one component fit in Figure 4, based on both the residuals shown in the figures and the χ^2_{ν} values listed in Table 1. More importantly, in the two component fit the D I and H I lines are self-consistent. The H-wall temperature derived from the Doppler parameter of the two component fit is $T = 49,000 \pm 9000 \text{ K}$, compared with $T = 29,000 \pm 5000 \text{ K}$ toward α Cen. It is worth noting, however, that the meaning of these measured temperatures is not entirely clear. The absorption component fits to the Lyman- α line use Voigt functions for the opacity profiles, which amounts to an implicit assumption that velocity distributions for each component are Maxwellian, but neutrals in the outer heliosphere are far from being in equilibrium and therefore do not have Maxwellian distributions (Baranov, Izmodenov, & Malama 1998; Lipatov, Zank, & Pauls 1998; Müller, Zank, & Lipatov 2000). Furthermore, the absorption components are integrated over a long line of sight through the heliosphere, resulting in even more complex velocity distributions.

There is a serious problem with the central velocity of the H-wall absorption inferred from the two-component fit. Heliospheric models all suggest substantial decelerations within the hydrogen

wall in the upwind direction (Baranov & Malama 1993, 1995; Pauls et al. 1995; Zank et al. 1996; Baranov et al. 1998; Lipatov et al. 1998; Müller et al. 2000), meaning the H-wall absorption should be significantly redshifted relative to projected velocity of the LIC for that line of sight, -25.1 km s^{-1} . The measured velocity, $v = -26.7 \pm 0.3 \text{ km s}^{-1}$, is only slightly redshifted relative to the G cloud absorption, and it is actually *blueshifted* relative to the LIC velocity. Figure 6a illustrates why this is the case. Non-LISM absorption exists on both the blue and red sides of the H I absorption feature, and the heliospheric component cannot be greatly redshifted away from the LISM absorption in order to account for the excess absorption on the blue side.

The only way the heliospheric absorption can have decelerations consistent with the models is for there to be yet another absorption component that accounts for the non-LISM absorption on the blue side of the line. Gayley et al. (1997) found this to be the case for the α Cen data as well when they made direct comparisons between the data and the H I absorption predicted by heliospheric models. Gayley et al. (1997) interpreted this to mean that the “astrosphere” of α Cen was responsible for the blueshifted non-LISM H I absorption. We propose that our Lyman- α data are also contaminated by astrospheric absorption.

Figure 2 shows the velocity vector of 36 Oph, which is computed from the radial velocity and proper motion information in Hirshfeld et al. (1996). From this 32.5 km s^{-1} stellar vector and the known 29.4 km s^{-1} G cloud vector, we can determine the interstellar wind vector in the rest frame of 36 Oph (dotted arrow in Fig. 2). We find that the wind speed relative to the star is 40 km s^{-1} and the line of sight toward the Sun is $\theta = 134^\circ$ from the upwind direction, meaning we are looking at the downwind portion of 36 Oph’s astrosphere.

Much of the heliospheric H I in downwind directions is formed by charge exchange between LISM neutrals and solar wind protons inside the heliopause, whereas the H-wall H I observed in upwind directions is created by charge exchange between LISM neutrals and heated LISM protons *outside* the heliopause. Another difference is that in the upwind direction, the H I in the H-wall is decelerated, but models suggest that for downwind directions the H I gas is *accelerated* relative to the LISM flow. One consequence of this is that heliospheric absorption will be redshifted relative to the LISM absorption in all directions. Likewise, astrospheric absorption will always be blueshifted. Izmodenov, Lallement, & Malama (1999) claim to have detected redshifted heliospheric absorption in a downwind direction toward the star Sirius, consistent with these theoretical expectations.

Therefore, it is not unreasonable to suppose that astrospheric material downwind from 36 Oph is responsible for the non-LISM absorption on the blue side of the Lyman- α absorption feature. Thus, in Figure 6b we present a three component fit to the Lyman- α line, the parameters of which are listed in Table 1. Because they are so highly blended, the three components must be constrained somehow to produce a unique fit. The LISM component is constrained the same as in the two component fit. Furthermore, we force the heliospheric and astrospheric absorption components to have velocities roughly consistent with model predictions.

Heliospheric models suggest an average deceleration of roughly 40% within the hydrogen wall in

the upwind direction, meaning the projected velocity toward 36 Oph should be $V_H = -0.6V_0 \cos \theta$, where $V_0 = 26 \text{ km s}^{-1}$ is the LISM flow velocity for the Sun and $\theta = 12^\circ$ is the angle of the line of sight relative to the upwind direction. Thus, $V_H = -15 \text{ km s}^{-1}$ for the heliospheric absorption. In downwind directions, the heliospheric models suggest accelerations of about 30% for the H I. Assuming this is the case for 36 Oph, the predicted velocity of the astrospheric absorption is then $V_H = V_{rad} + (1.3V_0 \cos \theta)$, where $V_{rad} = 1.0 \text{ km s}^{-1}$ is the stellar radial velocity, $V_0 = 40 \text{ km s}^{-1}$ is the LISM flow velocity relative to the star, and $\theta = 134^\circ$ is the angle relative to the upwind direction of the solar line of sight. Thus, $V_H = -35 \text{ km s}^{-1}$ for the astrospheric absorption. We arbitrarily assume uncertainties of $\pm 5 \text{ km s}^{-1}$ for both the estimated heliospheric and astrospheric velocities. Analogous to the procedure used in the two component fit, we perform many fits varying the LISM column density and the heliospheric/astrospheric velocities within the allowed error bars, which allows us to determine the best fit parameters and uncertainties quoted in Table 1.

Since the heliospheric component no longer has to account for the excess absorption on both the red and blue sides of the Lyman- α line, the column density and Doppler parameter are significantly lower than for the two component model (see Table 1). The column density ($\log N_H = 14.6 \pm 0.3$) is now consistent with that measured toward α Cen ($\log N_H = 14.74 \pm 0.24$), as is the temperature inferred from the Doppler parameter once the quoted uncertainties are considered ($T = 38,000 \pm 8000 \text{ K}$ for 36 Oph, $T = 29,000 \pm 5000 \text{ K}$ for α Cen).

The astrospheric component has a column density ($\log N_H = 14.7 \pm 0.3$) and Doppler parameter ($b = 26.0 \pm 3.0 \text{ km s}^{-1}$) very similar to that of the heliospheric component, with the Doppler parameter implying a temperature of $41,000 \pm 10,000 \text{ K}$. We would have expected temperatures somewhat higher than this for a downwind line of sight, based on the H I temperatures predicted by the hydrodynamic models (e.g., Müller et al. 2000). However, a direct comparison between the data and the absorption predicted by the models is needed to see if they are truly inconsistent.

The average LISM density toward 36 Oph is $n_H = 0.03 - 0.06 \text{ cm}^{-3}$. This is lower than the $n_H \approx 0.1 \text{ cm}^{-3}$ densities typically observed toward the nearest stars, including α Cen (Linsky et al. 2000). One possible explanation for this is that hot interstellar material without any neutral H occupies part of the line of sight, either in the foreground of the observed absorption between the LIC and G clouds; or beyond the G cloud, which would mean that 36 Oph lies outside the G cloud. However, if our detection of astrospheric H I is valid, the LISM around 36 Oph must necessarily contain H I, meaning 36 Oph must be within the G cloud. Furthermore, the existence of substantial G cloud material toward α Cen, which is only 1.3 pc away, suggests that a large gap between the LIC and G clouds toward 36 Oph is unlikely (see Fig. 2). Thus, the most likely explanation for the low average density is a negative density gradient within the G cloud toward 36 Oph. Wood & Linsky (1998) used similar reasoning to infer a density gradient within the LIC toward 40 Eri.

4. Summary

We have analyzed absorption features observed in HST/STIS spectra of the 5.5 pc line of sight to 36 Oph A. Our findings are summarized as follows:

1. Only one LISM absorption component is seen toward 36 Oph, with a velocity consistent with the flow vector of the G cloud. No absorption whatsoever is detected from the LIC, meaning the edge of the LIC must be very close. Because the line of sight is very close to the upwind directions of both the G and LIC clouds, the velocity of -28.4 km s^{-1} that we observe is very close to the actual flow speed of the observed material. The fact that this *projected* velocity is greater than the 26 km s^{-1} velocity of the LIC provides particularly strong evidence for the existence of faster G cloud material in that direction.
2. We estimate that the LIC D I column density must be less than $9 \times 10^{11} \text{ cm}^{-2}$ to explain why no LIC absorption is detected. This corresponds to $N_{\text{H I}} < 6 \times 10^{16} \text{ cm}^{-2}$ based on the known LIC D/H ratio (1.5×10^{-5}). Assuming a density of $n_{\text{H I}} = 0.1 \text{ cm}^{-3}$, the distance to the edge of the LIC is $d_{\text{edge}} < 0.19 \text{ pc}$. The Sun will reach the edge in $t_{\text{edge}} < 7400 \text{ yrs}$, based on the LIC velocity vector.
3. The temperature ($T = 5900 \pm 500 \text{ K}$) and relative abundances of D I, Mg II, and Fe II (e.g., $\text{D I/Mg II} = 0.9 \pm 0.4$) are within the error bars of the measurements made for the α Cen line of sight, which also samples G cloud material (LW96). These measurements suggest that the G cloud has a slightly lower temperature and less Mg and Fe depletion than the LIC. However, the nonthermal velocity toward 36 Oph, $\xi = 2.2 \pm 0.2 \text{ km s}^{-1}$, is higher than the α Cen measurement ($\xi = 1.25 \pm 0.25 \text{ km s}^{-1}$).
4. Using a Lyman- α bisector technique first described by Wood et al. (1996), we estimate a column density of $\log N_{\text{H}} = 17.85 \pm 0.15$ toward 36 Oph and a deuterium-to-hydrogen ratio for the G cloud of $\text{D/H} = (1.5 \pm 0.5) \times 10^{-5}$. The latter quantity is consistent with the LIC value of $\text{D/H} = (1.5 \pm 0.1) \times 10^{-5}$.
5. The average G cloud density toward 36 Oph is $n_{\text{H}} = 0.03 - 0.06$, significantly less than the $n_{\text{H}} \approx 0.1 \text{ cm}^{-3}$ densities typically observed toward the nearest stars, including α Cen within the G cloud. The most likely interpretation is that the G cloud H I density decreases toward 36 Oph.
6. The H I Lyman- α absorption line is redshifted and suggests a much higher temperature than the other lines. LW96 used a very similar discrepancy toward α Cen to argue for the presence of absorption from heated, decelerated material in the solar hydrogen wall. Our results strongly support this interpretation.
7. In two component fits to the H I Lyman- α line, the solar hydrogen wall component is not decelerated relative to the projected LIC velocity, which is a serious contradiction with theoretical

expectations, so we propose that absorption from astrospheric material around 36 Oph is responsible for some of the absorption on the blue side of the line. Thus, our best model of the Lyman- α absorption has three components: LISM (G cloud), heliospheric, and astrospheric. In the three component fits, the temperature and column density of the heliospheric absorption ($T = 38,000 \pm 8000$ K and $\log N_{\text{H}} = 14.6 \pm 0.3$) are consistent with the measurements made for the α Cen line of sight.

We would like to thank the anonymous referee for several helpful suggestions. Support for this work was provided by NASA through grant number GO-07262.01-99A from the Space Telescope Science Institute, which is operated by AURA, Inc., under NASA contract NAS5-26555.

REFERENCES

Baranov, V. B., Izmodenov, V. V., & Malama, Y. G. 1998, *J. Geophys. Res.*, 103, 9575

Baranov, V. B., & Malama, Y. G. 1993, *J. Geophys. Res.*, 98, 15157

Baranov, V. B., & Malama, Y. G. 1995, *J. Geophys. Res.*, 100, 14755

Bertaux, J. -L., Lallement, R., Kurt, V. G., & Mironova, E. 1985, *A&A*, 150, 1

Bertin, P., Vidal-Madjar, A., Lallement, R., Ferlet, R., & Lemoine, M. 1995, *A&A*, 302, 889

Dring, A. R., Linsky, J. L., Murthy, J., Henry, R. C., Moos, W., Vidal-Madjar, A., Audouze, J., & Landsman, W. 1997, *ApJ*, 488, 760

Gayley, K. G., Zank, G. P., Pauls, H. L., Frisch, P. C., & Welty, D. E. 1997, *ApJ*, 487, 259

Hirshfeld, A., Sinnott, R. W., & Ochsenbein, F. 1991, *Sky Catalogue 2000.0*, Vol. 1 (Cambridge: Cambridge Univ. Press)

Izmodenov, V. V., Lallement, R., & Malama, Y. G. 1999, *A&A*, 342, L13

Kimble, R. A., et al. 1998, *ApJ*, 492, L83

Lallement, R., & Bertin, P. 1992, *A&A*, 266, 479

Lallement, R., Bertin, P., Ferlet, R., Vidal-Madjar, A., & Bertaux, J. L. 1994, *A&A*, 286, 898

Lallement, R., Ferlet, R., Lagrange, A. M., Lemoine, M., & Vidal-Madjar, A. 1995, *A&A*, 304, 461

Lindler, D. 1999, CALSTIS Reference Guide (Greenbelt: NASA/LASP)

Linsky, J. L. 1998, *Space Sci. Rev.*, 84, 285

Linsky, J. L., Redfield, S., Wood, B. E., & Piskunov, N. 2000, *ApJ*, to appear Jan. 10

Linsky, J. L., & Wood, B. E. 1996, *ApJ*, 463, 254 (LW96)

Linsky, J. L., & Wood, B. E. 1998, in *Cosmic Chemical Evolution*, IAU Symposium 187 (Dordrecht: Kluwer), in press

Lipatov, A. S., Zank, G. P., & Pauls, H. L. 1998, *J. Geophys. Res.*, 103, 20631

Morton, D. C. 1991, *ApJS*, 77, 119

Müller, H. -R., Zank, G. P., & Lipatov, A. S. 2000, *J. Geophys. Res.*, in press

Pauls, H. L., Zank, G. P., & Williams, L. L. 1995, *J. Geophys. Res.*, 100, 21595

Piskunov, N., Wood, B. E., Linsky, J. L., Dempsey, R. C., & Ayres, T. R. 1997, *ApJ*, 474, 315

Quémérais, E., Sandel, B. R., Lallement, R., & Bertaux, J. -L. 1995, *A&A*, 299, 249

Redfield, S., & Linsky, J. L. 2000, *ApJ*, to appear May 10

Sahu, K. C., et al. 1999, STIS Instrument Handbook (Baltimore: STScI)

Witte, M., Rosenbauer, H., Banaszkiewicz, M., & Fahr, H. 1993, *Adv. Space Res.*, 13, 121

Wood, B. E., Alexander, W. R., & Linsky, J. L. 1996, *ApJ*, 470, 1159

Wood, B. E., & Linsky, J. L. 1998, *ApJ*, 492, 788

Woodgate, B. E., et al. 1998, *PASP*, 110, 1183

Zank, G. P. 1999, *Space Sci. Rev.*, 89, 413

Zank, G. P., Pauls, H. L., Williams, L. L., & Hall, D. T. 1996, *J. Geophys. Res.*, 101, 21639

Table 1. Fit Parameters^a

Ion	λ_{rest} ^b (Å)	Source of Absorption	v ^c (km s ⁻¹)	b (km s ⁻¹)	log N	χ^2_ν
One Component Fits						
Fe II	2600.173	LISM	-28.4 ± 0.4	2.12 ± 0.61	12.65 ± 0.25	0.41
Mg II ^d	2796.352	LISM	-27.9 ± 0.2	3.15 ± 0.25	13.05 ± 0.15	2.19
Mg II ^d	2803.531	LISM	-27.9 ± 0.2	3.15 ± 0.25	13.05 ± 0.15	2.19
D I	1215.339	LISM	-29.0 ± 0.2	7.33 ± 0.17	13.00 ± 0.01	1.12
H I	1215.670	LISM	-25.9 ± 0.1	14.34 ± 0.02	18.178 ± 0.002	2.30
Two Component Fits						
H I	1215.670	LISM	(-28.4)	(10.11)	(17.85 ± 0.15)	1.29
		Heliosphere	-26.7 ± 0.3	28.5 ± 2.5	15.08 ± 0.15	1.29
Three Component Fits						
H I	1215.670	LISM	(-28.4)	(10.11)	(17.85 ± 0.15)	1.25
		Heliosphere	(-15 ± 5)	25.0 ± 2.6	14.6 ± 0.3	1.25
		AstrospHERE	(-35 ± 5)	26.0 ± 3.0	14.7 ± 0.3	1.25

^aQuantities in parentheses are fixed rather than derived (see text for details).

^bIn vacuum.

^cCentral velocity in a heliocentric rest frame.

^dThe Mg II lines were fitted simultaneously and forced to have the same fit parameters.

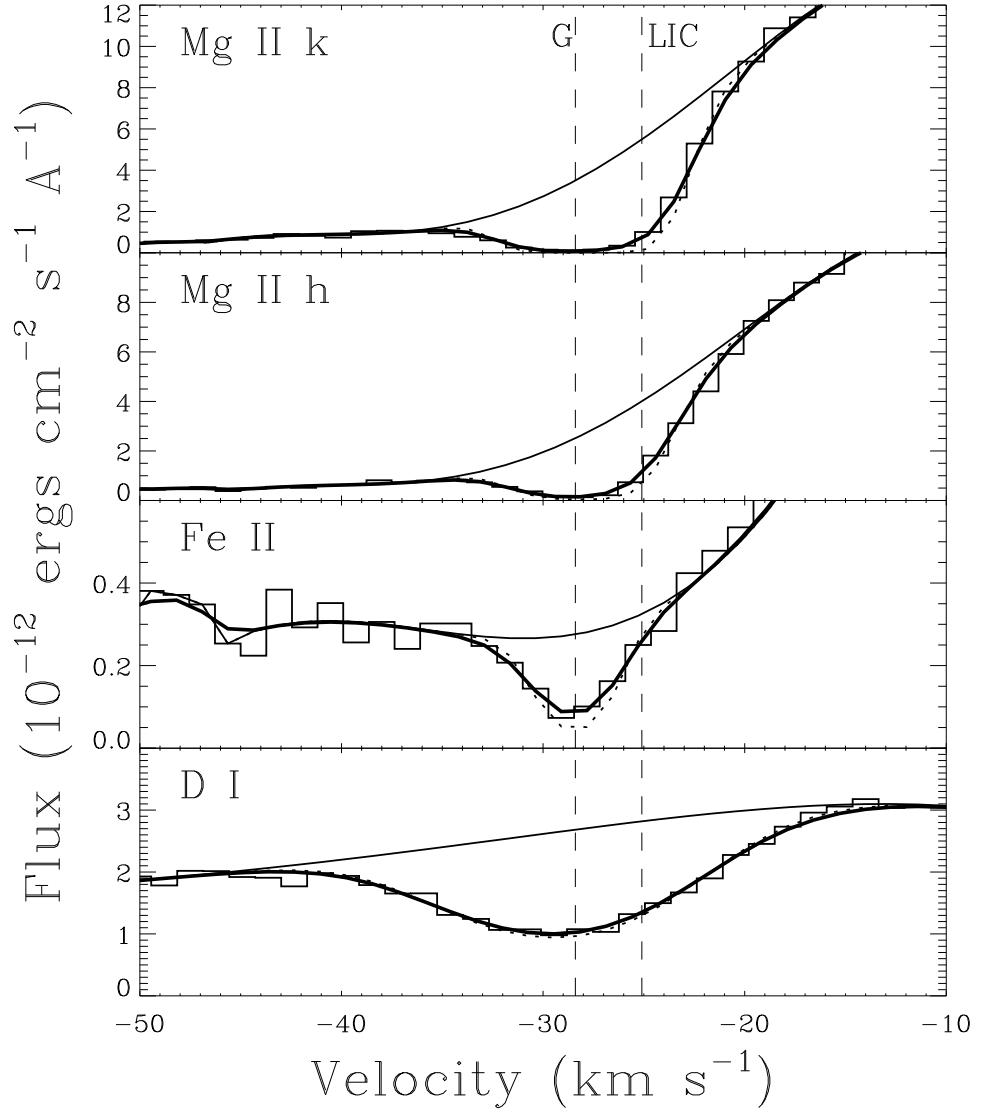


Fig. 1.— Single component absorption line fits to the following lines: Mg II k $\lambda 2796.352$, Mg II h $\lambda 2803.531$, Fe II $\lambda 2600.173$, and D I $\lambda 1215.339$. The dotted and thick solid lines are before and after instrumental broadening. The data are displayed on a velocity scale in a heliocentric rest frame. Dashed lines show the projected velocities of the LIC and G cloud flow vectors for the 36 Oph line of sight.

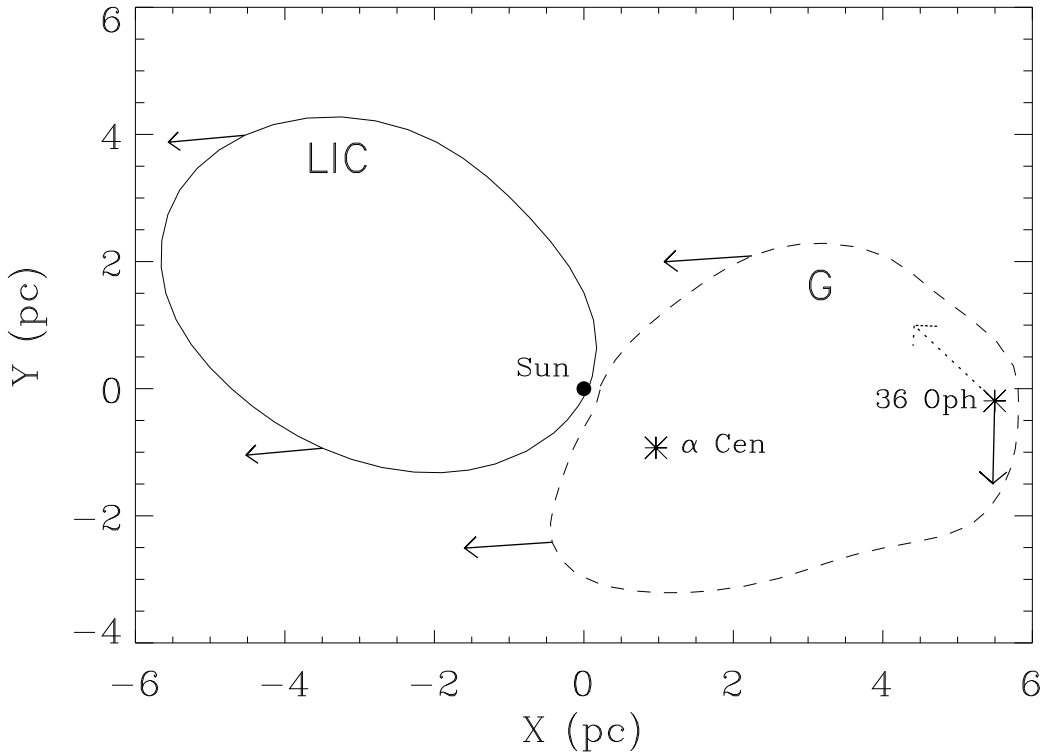


Fig. 2.— A map showing the locations of the Sun, α Cen, 36 Oph, the LIC (solid line), and G cloud (dashed line), projected into the Galactic plane, where Galactic Center is to the right. The LIC shape in the Galactic plane is from Redfield & Linsky (2000), while the G cloud shape is only a rough estimate. The solid arrows indicate the velocity vectors of the LIC, the G cloud, and 36 Oph relative to the Sun, with the length of the arrow being proportional to the speed. The dotted line indicates the G cloud vector in the rest frame of 36 Oph, thereby indicating the orientation of the star’s astrosphere. Note that the two stars and all the displayed vectors lie within 21° of the Galactic plane, so this two-dimensional map is not greatly misrepresentative of the actual three-dimensional situation.

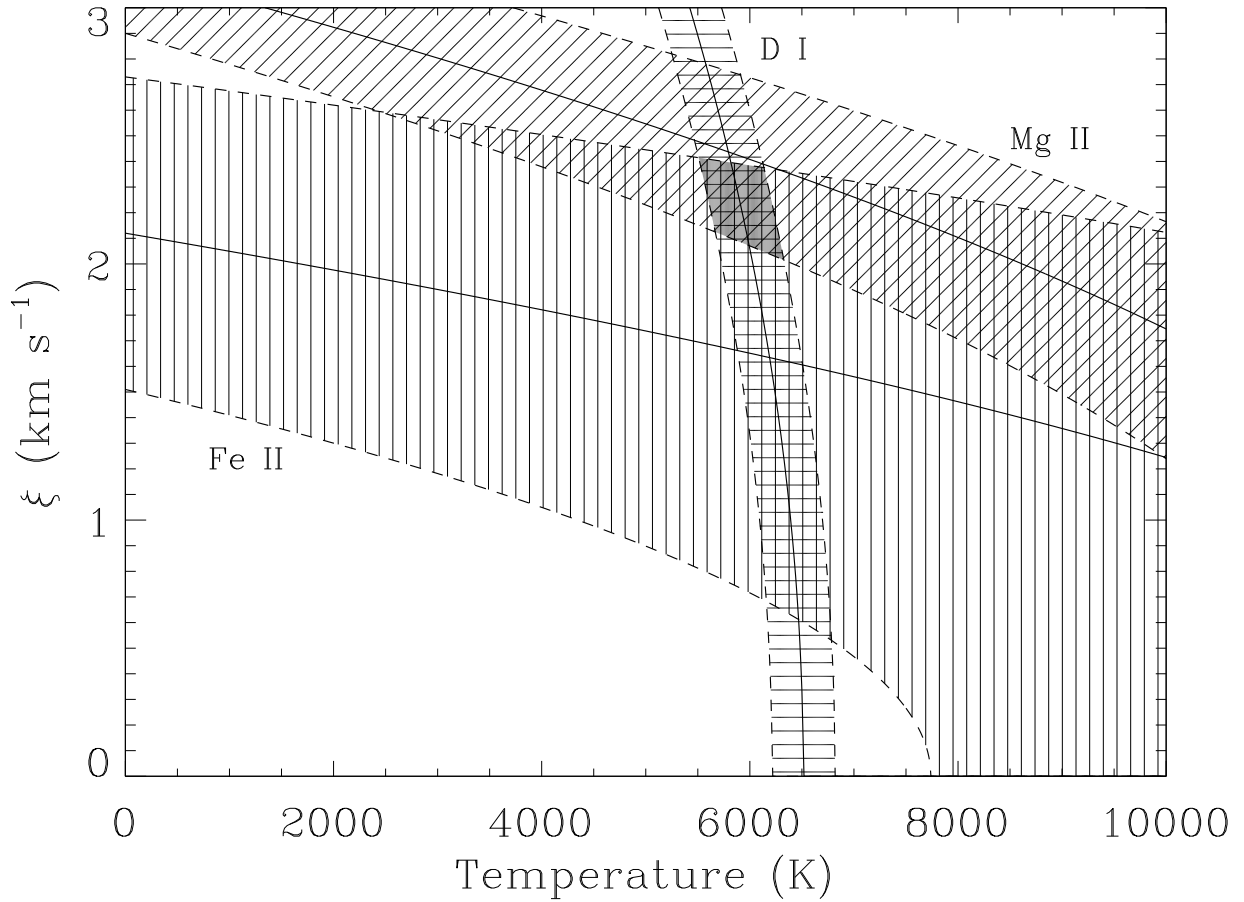


Fig. 3.— Nonthermal velocities (ξ) are plotted versus temperature, based on the Doppler parameters and their uncertainties measured from absorption lines of Fe II, Mg II, and D I (see Table 1). The shaded area where the three curves overlap indicates the actual temperature and ξ value of the interstellar material ($T = 5900 \pm 500$ K and $\xi = 2.2 \pm 0.2$ km s⁻¹).

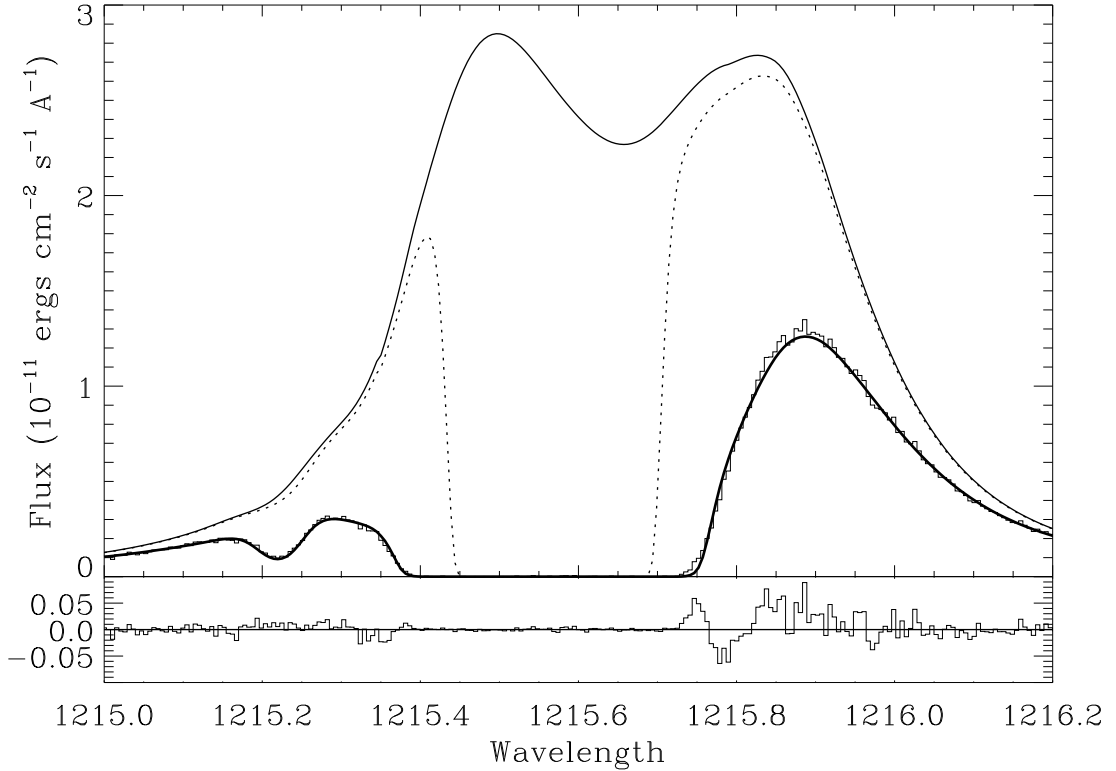


Fig. 4.— A single component fit (thick solid line) to the broad H I Lyman- α absorption line centered at 1215.6 \AA and the D I Lyman- α absorption at 1215.2 \AA , which are shown on a heliocentric wavelength scale. This fit is not realistic because the central velocity and temperature of the H I line are inconsistent with D I and the other LISM lines. The dotted line shows the LIC absorption associated with the upper limit for the LIC column density derived in the text ($N_{\text{H I}} < 6 \times 10^{16} \text{ cm}^{-2}$). Practically all of the absorption is well within the saturated core of the line, so LIC absorption will have no observable effect on the Lyman- α line.

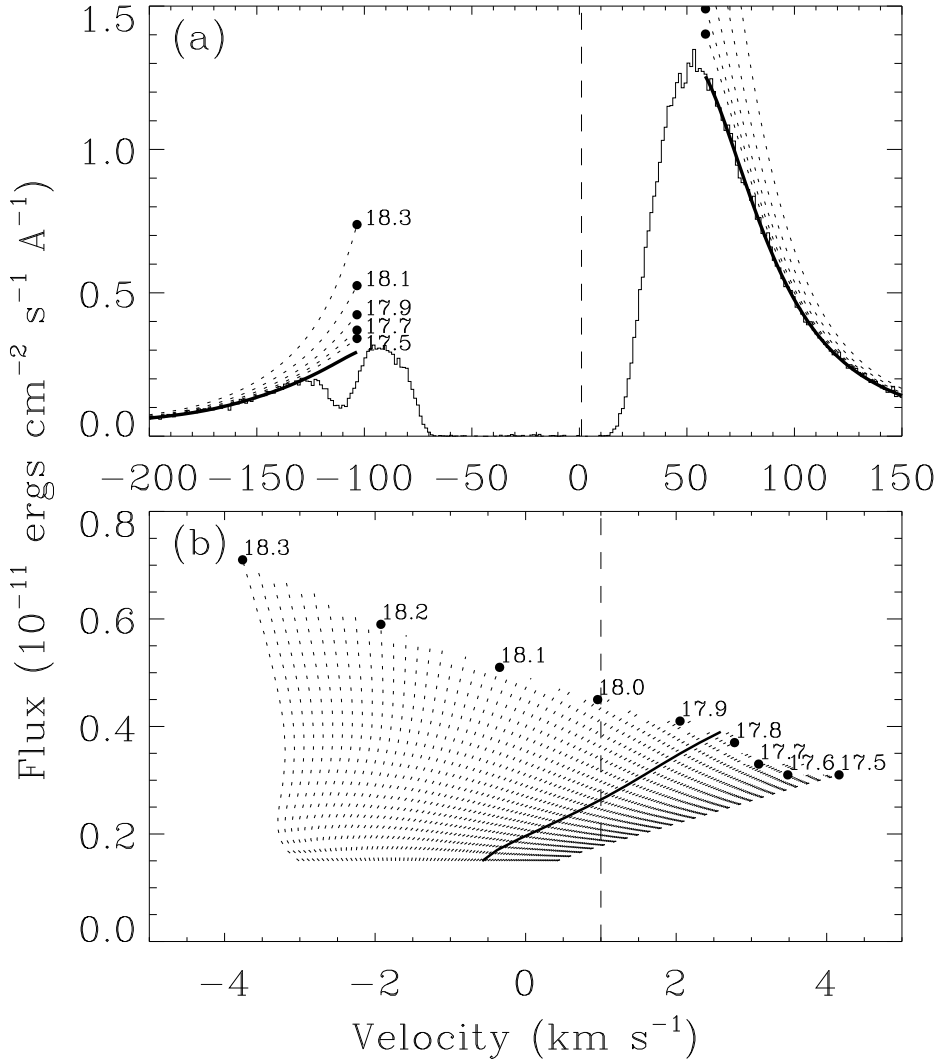


Fig. 5.— In (a), the wings of the unabsorbed stellar Lyman- α line are derived by extrapolating upwards from polynomial fits to the observed profile (thick solid lines) assuming five different LISM H I column densities in the range $\log N_{\text{H}} = 17.5 - 18.3$. The bisectors of Lyman- α wings computed in this fashion are shown in (b), as a function of $\log N_{\text{H}}$. When the correct value of $\log N_{\text{H}}$ is assumed, the bisector should be at the radial velocity of the star, which is shown as a dashed line in both panels. The thick line in (b) indicates the bisector that best matches the radial velocity, which corresponds to $\log N_{\text{H}} = 17.84$.

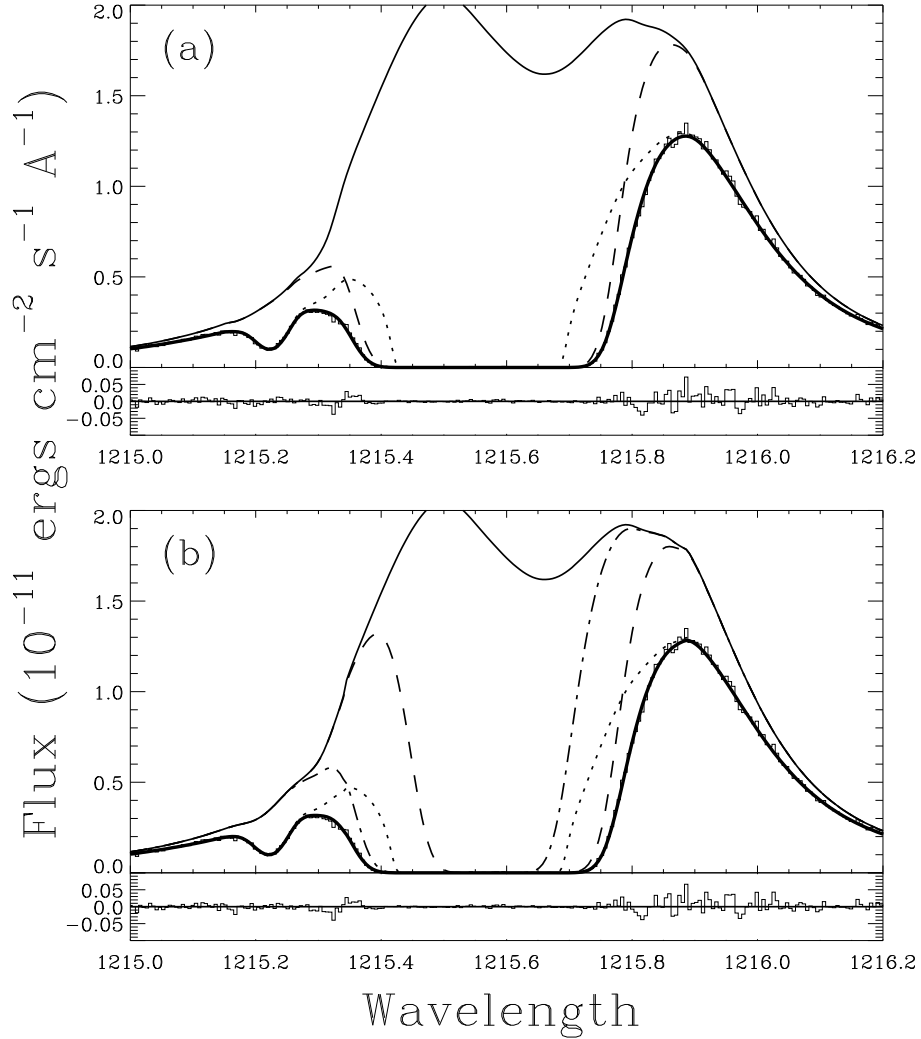


Fig. 6.— (a) A two component fit to the H I Lyman- α line, where the dotted line is LISM absorption and the dashed line is heliospheric hydrogen wall absorption. The thick solid line is the combination of the two components, which fits the data. Unlike the fit in Fig. 4, D I and H I are self-consistent in this fit. The spectrum is displayed in a heliocentric rest frame. (b) A fit similar to that in (a), but with the addition of a third component associated with absorption from hot astrospheric H I surrounding 36 Oph (dot-dashed line). We consider this to be our best model of the Lyman- α absorption (see text).